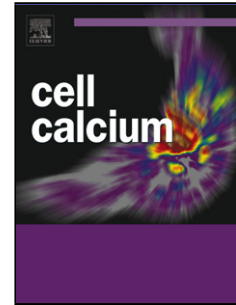


## Accepted Manuscript

Title: NAADP-dependent  $\text{Ca}^{2+}$  signaling regulates Middle East Respiratory Syndrome-Coronavirus pseudovirus translocation through the endolysosomal system

Authors: Gihan S. Gunaratne, Yang Yang, Fang Li, Timothy F. Walseth, Jonathan S. Marchant



PII: S0143-4160(18)30121-0  
DOI: <https://doi.org/10.1016/j.ceca.2018.08.003>  
Reference: YCECA 1970

To appear in: *Cell Calcium*

Received date: 9-7-2018  
Revised date: 7-8-2018  
Accepted date: 7-8-2018

Please cite this article as: Gunaratne GS, Yang Y, Li F, Walseth TF, Marchant JS, NAADP-dependent  $\text{Ca}^{2+}$  signaling regulates Middle East Respiratory Syndrome-Coronavirus pseudovirus translocation through the endolysosomal system, *Cell Calcium* (2018), <https://doi.org/10.1016/j.ceca.2018.08.003>

This is a PDF file of an unedited manuscript that has been accepted for publication. As a service to our customers we are providing this early version of the manuscript. The manuscript will undergo copyediting, typesetting, and review of the resulting proof before it is published in its final form. Please note that during the production process errors may be discovered which could affect the content, and all legal disclaimers that apply to the journal pertain.

# NAADP-dependent Ca<sup>2+</sup> signaling regulates Middle East Respiratory Syndrome-Coronavirus pseudovirus translocation through the endolysosomal system

*Running Title: TPC Inhibition Blocks MERS Translocation*

Gihan S. Gunaratne<sup>1</sup>, Yang Yang<sup>1</sup>, Fang Li<sup>2</sup>,  
Timothy F. Walseth<sup>1</sup>, Jonathan S. Marchant<sup>3#</sup>

<sup>1</sup>*Department of Pharmacology, University of Minnesota Medical School, MN 55455, USA*

<sup>2</sup>*Department of Veterinary and Biomedical Sciences, College of Veterinary Medicine, University of Minnesota, Saint Paul, MN 55108, USA*

<sup>3</sup>*Department of Cell Biology, Neurobiology and Anatomy, Medical College of Wisconsin, Milwaukee WI 53226, USA.*

#Correspondence: Jonathan S. Marchant, E-mail: [JMarchant@mcw.edu](mailto:JMarchant@mcw.edu)

Figures: 6

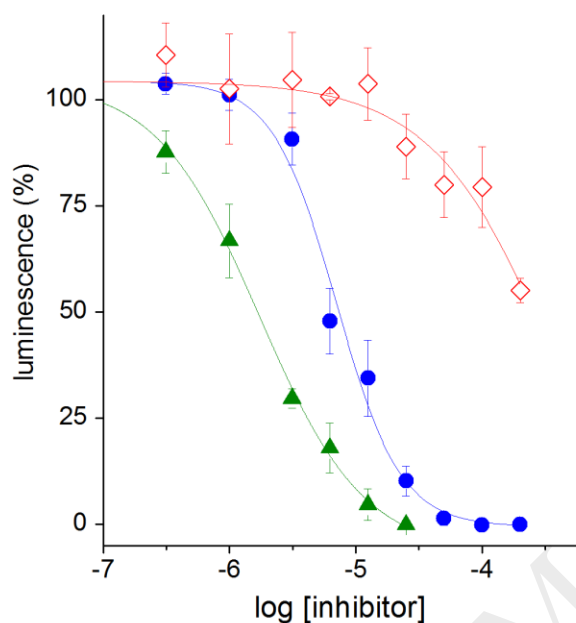
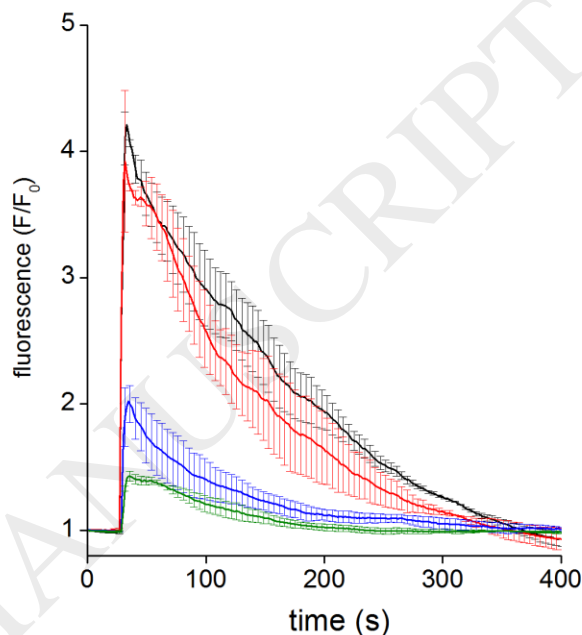
Tables: 1

Supplementary Figures: 6

Graphical abstract

## DRUG INHIBITION

MERS-CoV pseudovirus translocation

NAADP-evoked  $\text{Ca}^{2+}$  signal

## Highlights

- Nicotinic acid adenine dinucleotide phosphate (NAADP) releases  $\text{Ca}^{2+}$  from acidic organelles
- Middle East Respiratory Syndrome coronavirus (MERS-CoV) traffics through host-cell acidic organelles
- Blockers of NAADP action inhibited pseudotyped MERS-CoV infectivity
- Knockdown of two-pore channels (TPCs), a target of NAADP, also blocked MERS-CoV infectivity

**Middle East Respiratory Syndrome coronavirus (MERS-CoV) infections are associated with a significant mortality rate, and existing drugs show poor efficacy. Identifying novel targets/pathways required for MERS infectivity is therefore important for developing novel therapeutics. As an enveloped virus, translocation through the endolysosomal system provides one pathway for cellular entry of MERS-CoV. In this context,  $\text{Ca}^{2+}$ -permeable channels within the endolysosomal system regulate both the luminal environment and**

trafficking events, meriting investigation of their role in regulating processing and trafficking of MERS-CoV. Knockdown of endogenous two-pore channels (TPCs), targets for the  $\text{Ca}^{2+}$  mobilizing second messenger NAADP, impaired infectivity in a MERS-CoV spike pseudovirus particle translocation assay. This effect was selective as knockdown of the lysosomal cation channel mucolipin-1 (TRPML1) was without effect. Pharmacological inhibition of NAADP-evoked  $\text{Ca}^{2+}$  release using several bisbenzylisoquinoline alkaloids also blocked MERS pseudovirus translocation. Knockdown of TPC1 (biased endosomally) or TPC2 (biased lysosomally) decreased the activity of furin, a protease which facilitates MERS fusion with cellular membranes. Pharmacological or genetic inhibition of TPC1 activity also inhibited endosomal motility impairing pseudovirus progression through the endolysosomal system. Overall, these data support a selective, spatially autonomous role for TPCs within acidic organelles to support MERS-CoV translocation.

Keywords : NAADP,  $\text{Ca}^{2+}$  signaling, endosomes, lysosomes, infectious disease

## 1. INTRODUCTION.

Coronaviruses (CoV) are enveloped, single strand (+)RNA viruses that cause respiratory and enteric infections across a broad range of animal species. Several coronaviruses have recently emerged as zoonotic infections that cause life-threatening human disease, exemplified by the severe acute respiratory syndrome (SARS-CoV) epidemic in 2002/2003 as well as more recent clusters of infections caused by the Middle East Respiratory syndrome coronavirus (MERS-CoV). MERS-CoV is a lineage C beta-coronavirus first isolated in the summer of 2012 from a hospitalized patient in Saudi Arabia [1], and to date there have been >1,500 MERS cases worldwide. MERS-CoV infection causes symptoms of high fever and acute, progressive pneumonia in humans, and infection can be associated with a significant mortality rate (~30-50%)

in individuals with comorbidities [2, 3]. As no vaccine exists and trials of drugs and immune response modulators have demonstrated poor efficacy *in vivo*, there is considerable interest in identifying and optimizing novel therapies to resolve MERS-CoV infections [3, 4]. Therapeutic strategies encompass those targeting viral components as well as host-based processes that support MERS-CoV infectivity and replication [3, 4]. Consequently, resolution of the cell biology of MERS-CoV infection to illuminate the cellular infrastructure that controls viral entry, organelle passage and transfer into the cytoplasm for replication is of particular interest for evaluating new host targets with promise for development, or repurposing, of MERS-CoV therapeutics.

Research into the cell biology of MERS has shown that MERS-CoV particle entry is facilitated by interaction between the viral spike (S) protein and a specific host surface receptor, dipeptidyl peptidase 4 (DPP4, also known as CD26, [5]). Proteolytic priming of the spike protein promotes fusion of the viral envelope with host cell membranes, thus allowing successful translocation of the infectious viral genome into the host cell. Recent reports have demonstrated that such proteolytic priming and membrane fusion may occur either at the cell surface via the serine protease TMPRSS2 [6], or intracellularly in endocytic compartments via proprotein convertases such as furin (7). Following clathrin-mediated endocytosis, the virus traffics through the endolysosomal system where it is proteolytically activated by host proteases to mediate vesicular fusion and liberation into the cytoplasm [7, 8]. This subcellular translocation pathway affords opportunity for pharmacological intervention as generalized manipulations of endolysosomal function, through inhibition of endocytosis, cytoskeletal dynamics and bulk alkalization of acidic organelles, have been shown to impair MERS-CoV infectivity [7-10]. Such observations provide justification for pharmacological profiling of targets within acidic organelles to identify novel, more selective opportunities to impair MERS-CoV translocation through the endolysosomal system.

Ion channels of the two-pore channel (TPC1, TPC2) and mucolipin family (e.g. TRPML1) reside within the endolysosomal system where they regulate endolysosomal microenvironment and trafficking functions [11, 12]. As MERS-CoV translocation and release into the cytoplasm requires the interplay with the endolysosomal milieu [7, 8], the ability of these  $\text{Ca}^{2+}$ -permeable channels to acutely regulate luminal ionic composition and pH promotes their consideration as potential therapeutic targets. Manipulation of endolysosomal ion channel function has been shown to impact endolysosomal morphology and homeostatic trafficking in a variety of cell types [13-20]. Pharmacological manipulation of these channels may therefore permit a defer approach for impairing MERS-CoV translocation than more generalized perturbations of endolysosomal function. Of special relevance is the recent discovery that the natural product tetrandrine acts as a potent blocker of both TPC activity and Ebola infectivity, reducing viral titers in the serum of infected mice [21]. The efficacy of tetrandrine related to interference with a late step in Ebola virus translocation, possibly by preventing viral-endosome membrane fusion from within TPC2-positive structures [21], or by interfering with a TPC2-driven late endosome/lysosome maturation process [22]. Such data provide impetus for considering TPCs as druggable targets for combating a potentially broad range of infectious pathogens that must traverse, or reside within, the acidic  $\text{Ca}^{2+}$  store milieu. Here, we use both pharmacological and molecular approaches to address this concept in the context of MERS-CoV infectivity, as the contribution played by endolysosomal channels in facilitating MERS-CoV translocation is currently unknown.

## 2. MATERIALS AND METHODS.

*2.1 Drugs and Molecular reagents* – Chemicals were sourced as follows: hernandezine, metocurine, thaligine (isofangchinoline), cycleanine (Specs chemistry database), YM201636 (InvivoGen), Gly-Phe-B-naphthylamide (GPN), trans-Ned-19, (Santa Cruz Biotechnology), ARN14988 (Echelon Biosciences), D-NMAPDD and FTY720 (Cayman Chemicals), fumonisin  $\beta$ 1 (Enzo Life Sciences), N,N'-[1,2-ethanediylbis(oxy-2,1-phenylene)]bis[N-[2-[(acetyloxy)methoxy]-2-oxoethyl]]-, bis[(acetyloxy)methyl] ester (BAPTA-AM, Biotium). All other ligands were purchased from Sigma Aldrich. NAADP was synthesized from nicotinamide adenine dinucleotide phosphate as previously described [23]. pEGFP-N3 was from Clontech. Anti-GFP (rabbit polyclonal), anti-Rhodopsin C9 (mouse monoclonal), anti-HA (rabbit polyclonal) and anti-GAPDH (rabbit polyclonal) antibodies were from Santa Cruz. Plasmids encoding TPC1-GFP, TPC1[L273P]-GFP, TPC2-GFP, TPC2pm and Rab7a-GFP were from Sandip Patel (UCL) and have been described previously [14, 24, 25]. pGP-CMV-NES-GCaMP6M was from Douglas Kim (Addgene plasmid #40754), TMPRSS2 was from Tom Gallaher (Loyola) and EGFP-Rab7a[Q67L] from Qing Zhong (Addgene plasmid #28045 and #28049, respectively). Silencer Select siRNAs targeted against Tpcn1, Tpcn2, and Mcoln1 and non-targeting negative control siRNA were purchased from Invitrogen. siRNA sequences were: Tpcn1 siRNA#1 – GCGUCUUCUUCAUCGUGUA, Tpcn1 siRNA#2 – GGCUACUAUUAUCUCAUA; Tpcn2 siRNA#1 – CGGUAUUACUCGAACGUAU, Tpcn2 siRNA#2 – ACAGAAGUGUGGUUAAAGA; Mcoln1 siRNA#1 – CCUUCGCCGUCGUCUCAA, Mcoln1 siRNA#2 – GAUCACGUUUGACAACAAA; Smpd1 siRNA#1 – UCACAGCACUUGUGAGGAAtt, Smpd1 siRNA#2 – CUACCUACAUCGGCCUUAAtt; Asah1 siRNA#1 – CCUUGAUAGAUGUUACCAAtt, Asah1 siRNA #2 – GCAGUCCAUGGUACACCAtt; Cers2 siRNA#1 – GGCTATTACTTCTTCAATTt, Cers2 siRNA#2 – GCATTGCCTCTGATGTCAAtt.

*2.2 Cell Culture and transfection* – HEK293 (human embryonic kidney) were sourced from ATCC. Huh7 (human liver) cells and U-2OS (human bone osteosarcoma) were gifts from Charles M. Rice (Rockefeller) and Eugen Brailoiu (Temple) respectively. Cell lines were maintained in DMEM (Invitrogen) supplemented with 10% fetal bovine serum (FBS, Invitrogen), 100 units/ml penicillin and streptomycin, 292µg/ml L-glutamine (Invitrogen) and cultured at 5% CO<sub>2</sub> and 37°C. Transfection of plasmid DNA was performed in 6-well dishes (Nunc) using Lipofectamine® 2000 (Invitrogen). Cells were transfected using 750ng of each DNA construct, using a 1:3 DNA:Lipofectamine® 2000 ratio. Complexes were prepared in Opti-MEM (Invitrogen) and added to cells in DMEM without FBS or antibiotics. Complexes were removed after 6hrs and media was exchanged with DMEM containing FBS. Transfection of siRNA was performed in 6-well dishes using INTERFERin (Polyplus) according to the vendor's protocol. Cells were passaged three times to maintain subconfluency over the course of 5 days during which time siRNA:INTERFERin complexes were replenished to ensure protein knockdown. Knockdown was validated by RT-PCR for positive and negative controls.

*2.3 Production of MERS-CoV pseudovirus and cellular translocation assay* – MERS pseudovirus manipulations were carried out as described previously [26, 27]. MERS-CoV-spike-pseudotyped retroviruses expressing a luciferase reporter gene were prepared by co-transfecting HEK293T cells with a plasmid carrying Env-defective, luciferase-expressing HIV-1 genome (pNL4-3.luc.RE) and a plasmid encoding MERS-CoV spike (S) protein. The S protein has previously been shown to be necessary and sufficient to facilitate MERS-CoV cell entry. M.ERS-pseudovirus particles were harvested from supernatant 72hrs after transfection. Huh7 cells, which express hsDPP4 endogenously [26], were used to resolve the effects of drugs on MERS-pseudovirus translocation. Huh7 cells were seeded into 96-well plates (Midwest Scientific) at a concentration of 1x10<sup>4</sup> cells/well. The following day, cells were pre-incubated with individual drugs (10µM final concentration) for 1 hour prior to MERS-pseudovirus addition. Cells were incubated (5%

CO<sub>2</sub>/37°C) for an additional 5 hours in the presence of drug and pseudovirus. After 6hrs, the culture media was replaced with complete DMEM and cells were incubated for a further 60hrs. Cells were then washed 3 times with DPBS (Invitrogen) and assayed for luciferase activity. Cells were lysed in 80µl lysis buffer (Promega) per well, and 40µl of lysate was transferred to solid-white 96-well plates (Corning) and mixed with 40µl of luciferase substrate (Promega). Luminescence (relative luminescence units, RLUs) were measured using a GloMax-multi detection system (Promega). Luminescence values are reported relative to levels measured in cells treated with virus alone, background corrected by luminescence values in cells unexposed to virus, except where indicated. For cell viability assays, Huh7 cells were lysed 60 hrs post drug treatment, using cell lysis buffer (Promega). Lysates were transferred to solid white 96-well plates to be screened in an ATP-based viability assay (CellTiter-Glo 2.0, Promega) according to the vendor's protocol. Finally, for molecular manipulations, HEK293 cells (1.5x10<sup>4</sup> cells/well) were used owing to higher transfectability. Extra samples were harvested, for immunoblotting or RNA extraction, from the same samples used to study pseudovirus infectivity.

*2.4 Immunofluorescence microscopy* – For colocalization analyses, Huh7 cells or HEK293 cells (co-transfected with hsDPP4-HA) were transfected with plasmids encoding GFP-tagged proteins of interest. One day after transfection, cells were incubated with MERS-pseudovirus (2hrs, 4°C) to allow adsorption of the pseudovirus particles to hsDPP4 receptors at the cell surface. After a brief incubation (45mins, 5% CO<sub>2</sub>/37°C), cells were then fixed in methanol. Samples were blocked with 3% BSA and incubated with primary antibody (1:250 dilution) overnight at 4°C. Cells were incubated with an Alexa Fluor-conjugated secondary antibody (Invitrogen) for 1hr at room temperature (5µg/ml). Cells were imaged on an Olympus IX81 inverted microscope using a Plan-Apochromat 60x/1.42 oil-immersion objective, using a spinning disk confocal unit (Yogogawa CSU-X1). Images were captured using a Clara interline CCD camera (Andor).

*2.5 NAADP Microinjection experiments* – U2OS cells were transfected with plasmid encoding GCaMP6M two days prior to microinjection experiments. One day post-transfection,  $1 \times 10^6$  cells were seeded onto collagen coated MatTek dishes. For microinjection experiments, dishes were mounted on an Olympus IX81 inverted microscope equipped with a piezo nanopositioning stage (Prior Scientific). Cells were perfused with  $\text{Ca}^{2+}$ -free Hank's Balanced Salt Solution (Thermo Scientific) at a rate of 0.5ml/min. Isolated U2OS cells expressing GCaMP6M identified by fluorescence were selected for injections. Cell morphology was assessed by acquiring z-stack images and reconstructing three-dimensional models of each cell to be injected. Regions that were not relatively close to the nucleus or cell periphery were targeted for injection sites. Femtotip (Eppendorf) injection pipettes were backfilled with intracellular buffer (110mM KCl, 10mM NaCl, 20mM HEPES, pH 7.2) containing either vehicle or NAADP (100nM), and positioned using an Injectman-4 (Eppendorf) micromanipulation system. Cells were injected at a z-position approximately 70% of the cell thickness at the site of injection using a Femtojet4i (Eppendorf). Injection parameters were 85hPa injection pressure, 40hPa compensation pressure, 0.5s injection duration,  $45^\circ$  injection angle, and 600um/s injection speed. Cells to be injected were imaged ( $\lambda_{\text{ex}}=488\text{nm}$ ,  $\lambda_{\text{em}}=514 \pm 15\text{nm}$  bandpass) using a Plan-Apochromat 60x/1.42 objective, and fluorescence changes were monitored using a Yokogawa spinning disk confocal (CSU-X- M1N), and an Andor iXon Ultra 888 EMCCD camera. Image acquisition and data collection was done using Metamorph version 7.10.

*2.6 Immunoblotting* – Cells were lysed at  $4^\circ\text{C}$  on a nutating mixer in ice-cold lysis buffer consisting of PBS (Invitrogen), 1% Triton X-100 (Fluka), 1x cOmplete protease inhibitors (Roche). Protein concentration was determined by Bradford assay (Pierce), and 25 $\mu\text{g}$  of protein was loaded onto 'Any-kD' mini-PROTEAN TGX gels (BioRad) for SDS-PAGE. After electrophoresis, protein was transferred to nitrocellulose membranes using a TransBlot Turbo (BioRad) semi-dry transfer machine. Membranes were blocked for 1hr at room temperature in 5% milk in PBS supplemented

with 0.1% Tween-20, prior to addition of primary antibody (1:1000 dilution for anti-GFP and anti-HA antibodies, 1:2000 dilution for anti-GAPDH antibody) and overnight incubation at 4°C. The following day, membranes were incubated with IRDye secondary antibodies (1:5000 dilution, LI-COR) for 1hr at room temperature. Signals were detected using a LI-COR Odyssey Imaging system.

*2.7 RNA isolation and RT-PCR* – RNA was isolated from HEK293 cells after siRNA treatment using TRIzol (Invitrogen) according to the vendor's protocol. RNA aliquots were frozen at -80°C prior to RT-PCR analysis. RT-PCR evaluation of knockdown of mRNA of interest was assessed using the following primers: Tpcn1 F – GACCACAGCCAATTTCCCAG, Tpcn1 R – CGCTTGTGCAGTAGCAAAGA. Tpcn2 F – ACGGACTTTGAGCTTCACCAT, Tpcn2 R – CGAACAGGTAACCCTTCACAGA. Mcoln1 F – GGTGCAGCTCATCCTGTTTG, Mcoln2 R – ACCACGGACATACGCATACC. Smpd1 F – CTGCGCACCTCAGAATTGG, Smpd1 R – TGTCTCCTCGATCCTCAGCA, Asah1 F – CCTTCAGGACCAACGTACAGAG, Asah1 R – AAAAGGGCCAGGAAAGTTGC, Cers2 F – TTCTTTGAGCTGTACGTGGCT, Cers2 R – GCTGGCTTCTCGGAACTTCT, Gapdh F – TGCACCACCAACTGCTTAG, Gapdh R – GCATGGACTGTGGTCATGAG. Superscript III One-Step RT-PCR System with Platinum Taq (Invitrogen) was used to convert mRNA to cDNA and amplify samples in a single reaction. semi quantitative RT-PCR reactions (35 cycles) were multiplexed to amplify GAPDH and mRNA of interest simultaneously. PCR products were separated on a 2% agarose gel. Gels were imaged using a myECL (Thermo Fisher) and quantified by densitometry (ImageJ).

*2.8 Protease activity assays.* Intracellular furin activity was detected using a fluorogenic substrate, Boc-Arg-Val-Arg-Arg-7-amino-4-methylcoumarin (Boc-RVRR-AMC, Enzo Life Science). For pharmacological assays, Huh7 cells were cultured in the presence of vehicle or drug for 4hrs, or were left untreated. For knockdown assays, HEK293 cells were treated with the indicated siRNAs

as described above. Cells were washed in PBS, and lysed in cold PBS containing 1% triton X-100 and phosphatase inhibitors (Thermo Scientific). Protein concentration was determined by Bradford assay and diluted to 1 $\mu$ g/ $\mu$ l, 100 $\mu$ l was dispensed into individual wells in a clear-bottom, black walled 96-well plate (Cellstar). Furin substrate (10 $\mu$ M final concentration) was added to each well. To test for direct inhibition of furin activity, fangchinoline was added immediately before addition of furin substrate. Fluorescence was monitored using a Tecan M1000 plate reader at 37°C,  $\lambda_{Ex}$ =360-380nm,  $\lambda_{Em}$ =440-460nm.

*2.9 Endosomal motility assays.* For baseline endosomal motility measurements, Huh7 cells were cultured in the presence of 200 $\mu$ g/ml FITC-Dextran (Sigma) in complete media for 20min to allow endocytic uptake, before rinsing with PBS and imaging. Motility of endosomes expressing wild-type or dominant-negative TPC1 was done by transfecting Huh7 cells with the indicated GFP-tagged constructs and imaging GFP fluorescence. Assessment of pharmacological inhibition of endosomal motility was performed by treating Huh7 cells with the indicated compounds for 1hr at 37C prior to loading with FITC-dextran as described above. Cells were imaged on an Olympus IX81 microscope equipped with a Piezo Nanopositioning stage (Prior Scientific) using a PlanApochromat 60x/1.42 oil-immersion objective, using a spinning disk confocal unit (Yokogawa, CSU-X1) and an iXon 888 EMCCD camera (Andor). Endosomal structures were tracked by acquiring a series of z-stacks over a time course of 5 minutes. Maximum intensity projections of z-stacks at each time point were generated, and the Track Particles Addon was used in Metamorph to assess movement of endosomes and produce trajectory plots.

### 3.0 RESULTS

*3.1 The endolysosomal milieu impacts MERS-CoV pseudovirus translocation.* MERS pseudovirus entry and subcellular trafficking was monitored using a luciferase assay [26, 27] in which the pseudovirus genome was engineered to encode a luciferase that generates a luminescence signal after release into the cytoplasm, thereby reporting the efficiency of subcellular translocation events (receptor binding, internalization, endolysosomal trafficking, cytoplasmic release; Figure 1A). To validate this assay in our hands, preliminary experiments were performed following infection in Huh7 cells, using drugs previously shown to inhibit specific steps required for MERS infectivity.

Ouabain, a cardiac glycoside inhibitor of early coronavirus internalization events [9] inhibited MERS-CoV pseudovirus translocation when applied prior to pseudovirus addition (Figure 1B). Similarly, chlorpromazine - an inhibitor of clathrin-mediated endocytosis [28] - resulted in lower luminescence values. Inhibition was also observed with several drugs that elevate endolysosomal pH, including chloroquine, the lysomotropic weak base  $\text{NH}_4\text{Cl}$  and bafilomycin A1, an inhibitor of the vacuolar-type  $\text{H}^+$ -ATPase, [7, 8, 10, 27, 29]. The cell permeable  $\text{Ca}^{2+}$ -chelator BAPTA-AM also inhibited MERS-CoV pseudovirus translocation (Figure 1B). Bafilomycin was a particularly effective inhibitor of MERS-CoV pseudovirus trafficking, reducing luminescence signal to background levels (Figure 1B, [8]). This inhibitory effect was ablated when bafilomycin application was delayed 5 hours after viral addition (Figure 1C). The inhibitory action of BAPTA-AM was similarly time-sensitive (Supplementary Figure 1), both results demonstrating that MERS-CoV pseudovirus translocation is rapid and regulated contemporaneously by the endolysosomal microenvironment.

*3.2 Endolysosomal ion channels regulate MERS-CoV pseudovirus translocation.* Endolysosomal ion channels, including the two-pore channel family (TPC1 and TPC2) and the mucolipin family (TRPML) of TRP channels (Figure 1A), regulate organellar microenvironment and trafficking

dynamics [11, 30, 31]. To examine their impact on MERS-CoV pseudovirus translocation, we applied both molecular and pharmacological tools to modulate individual channel activity. For RNAi analyses, constructs were expressed in HEK293 cells to capitalize upon the high transfectability of this cell line. Experiments assaying MERS infectivity in HEK293 cells also necessitated co-expression of the MERS-CoV entry receptor dipeptidyl peptidase 4 (hsDPP4, [5]) owing to low endogenous hsDPP4 expression: luminescence levels were low in the presence of pseudovirus and endogenous DPP4 alone and expression of hsDPP4 resulted in ~5-fold enhancement of luminescence signal (Figure 2A, [29]). Co-expression of a GFP control plasmid did not alter infectivity levels (Figure 2A). As negative and positive controls, transfection of a dominant negative Rab construct (Rab5a[S34N]) which impairs endocytic activity depressed MERS-CoV pseudovirus infectivity, whereas a constitutively active Rab variant (Rab7a[Q67L]) potentiated MERS-CoV pseudovirus infectivity (Figure 2A).

Loss of function analyses were performed using multiple siRNAs targeting individual endolysosomal  $\text{Ca}^{2+}$  channels. Discrete siRNAs targeting TPC1, TPC2 and TRPML1 were transfected into cells and infectivity assays performed 1 day after the final transfection. Whereas two discrete control siRNAs, or dual siRNAs targeting TRPML1 had little effect in this assay, knockdown of endogenous TPC1 or TPC2 markedly inhibited MERS translocation (Figure 2A). Co-transfection of TPC1 and TPC2 siRNA did not enhance this inhibitory effect (Figure 2A). The penetrance of knockdown attained with these siRNAs was evaluated by RT.PCR in the same set of transfections used for the pseudovirus infection assay. Representative gels are shown (Figure 2B) together with associated densitometry from all additional experiments evidencing knockdown of individual channels (Figure 2B). Overexpression of TPC isoforms, a manipulation known to perturb endolysosomal trafficking, also impaired MERS-CoV pseudovirus translocation (Figure 2A). Overexpression of TRPML1 was without effect (Figure 2A). This inhibitory effect was dependent on appropriate subcellular targeting of the active channel as overexpression of a

functional TPC2 channel rerouted from acidic  $\text{Ca}^{2+}$  stores to the cell surface (TPC2pm, [25]) by deletion of the  $\text{NH}_2$ -terminal lysosomal targeting motif did not inhibit MERS-CoV pseudovirus infectivity (Figure 2A). Moreover, the inhibitory action of these manipulations was not caused by alterations in DPP4 expression, as similar DPP4 expression levels were observed across all conditions (Supplementary Figure 2).

Colocalization between TPC isoforms and the MERS-CoV spike protein was then examined by immunofluorescence staining against the C9-epitope tagged spike protein. These experiments were performed using Huh7 cells owing to the fact that this cell line expresses higher endogenous levels of hsDPP4 (~18-fold, compared with HEK293 cells [7]). This obviates the need for hsDPP4 transfection and allows examination MERS-CoV pseudovirus trafficking in a native cell line. While no signal was evident in Huh7 cells unexposed to pseudovirus, MERS-CoV spike protein could be resolved in vesicular structures in cells previously incubated with pseudovirus (2hr, 4°C) and fixed 45min after a 37°C incubation (Figure 3). Co-transfection with Rab5-GFP or Rab7-GFP evidenced MERS CoV spike protein co-localization within a subset of both Rab5-GFP and Rab7-GFP positive vesicles (Supplementary Figure 3). Expression of TPC constructs (TPC1-GFP, TPC2-GFP) evidenced colocalization between the MERS CoV spike protein with both TPC2 (biased toward lysosomes [24, 32]) and TPC1 (biased toward endosomes [24, 32]) in all samples examined (Figure 3). Colocalization between MERS-CoV spike protein and GFP-TRPML1 was also observed (Figure 3). Collectively these data are consistent with MERS pseudovirus translocation through TPC positive endolysosomal organelles (Figure 3), with the properties and/or dynamics of these structures that are permissive for MERS-CoV pseudovirus translocation being regulated by endogenous TPC activity (Figure 2).

*3.3 TPC inhibitors block MERS Co-V pseudovirus translocation.* Can TPC modulators attenuate MERS trafficking through the endolysosomal system? TPC activity is regulated by the

endolysosomal phospholipid PI(3,5)P<sub>2</sub>, as well as the potent Ca<sup>2+</sup> releasing second messenger NAADP (Figure 1A). Lipid modulators, NAADP antagonists and a range of voltage-operated ion channel blockers have all been shown to regulate TPC activity [18, 21, 24, 32-36]. To examine the effects of TPC regulators on MERS-CoV pseudovirus translocation, a fixed concentration (10µM) primary drug screen was performed in Huh7 cells, with the goal of identifying plasma membrane-permeable compounds with inhibitory activity on MERS-CoV pseudovirus translocation. The effects of NAADP antagonists/pore blockers (Figure 4) and lipid modulators (Supplementary Figure 6) are described in turn below.

TPCs show affinity for a broad range of voltage-operated channel ligands, possibly reflecting their ancient evolutionary pedigree as antecedents of four domain voltage-gated ion channels [33]. Consistent with these observations, several Na<sup>+</sup> channel blockers (procaine, benzocaine) and voltage-operated Ca<sup>2+</sup> antagonists (verapamil, nifedipine and nimodipine) attenuated MERS-CoV pseudovirus translocation (Figure 4A). Of particular relevance were the effects of bisbenzylisoquinoline alkaloids, compounds consisting of dual benzylisoquinoline moieties linked together by ether bridge(s) (Figure 4B, Supplementary Figure 4). These compounds are of interest in light of the recent discovery that tetrandrine, a bisbenzylisoquinoline alkaloid natural product, blocked TPC activity and potently inhibited Ebola virus infectivity *in vitro* and *in vivo* [21]. Therefore, we screened several bisbenzylisoquinoline alkaloids from two different groupings (Figure 4B) – tubocurarine-like ligands where the isoquinoline pairs were non-adjacent within the bisbenzylisoquinoline ring structure (abab, 'head-to-tail'), and tetrandrine-like ligands, where the isoquinoline groups are directly conjoined (aabb, 'head-to-head and tail-to-tail'). These two groups are discriminated by shading intensity in Figures 4A&B and structures of individual compounds are provided in Supplementary Data (Supplementary Figure 4). Several structure-activity insights were clear from the screening dataset. First, the tubocurarine-like bisbenzylisoquinolines (tubocurarine, cycleanine, metocurine) were considerably less effective compared to the

tetrandrine-like ligands (tetrandrine, thaligine and fangchinoline) which strongly impaired MERS-CoV pseudovirus translocation (Figure 4A&B). Second, the presence of individual methoxy moieties around the compound ring structure markedly influenced the penetrance of individual ligands, with examples of ring substitutions that preserved (fangchinoline, thaligine) or decreased (berbamine, herandezine) drug effectiveness relative to the anti-Ebola prototype tetrandrine. Finally, fangchinoline, and the stereoisomer thaligine ('isofangchinoline') were the most effective compounds at inhibiting MERS translocation in these assays. Compounds from the initial screen were further evaluated in full concentration-response relationships for inhibition of MERS-CoV pseudovirus infectivity (Figure 4C). The relative sensitivities to screened compounds – fangchinoline ( $IC_{50}=1.7\pm 0.1\mu M$ ) > tetrandrine ( $IC_{50}=7.0\pm 0.8\mu M$ ) > berbamine ( $IC_{50}=29.2\pm 7.0\mu M$ ) were consistent with the primary screen (fixed concentration,  $10\mu M$ ). Cellular viability was measured in parallel and used to calculate a 'selectivity index' for these selected compounds. Calculation of the selectivity index (cytotoxic concentration 'CC<sub>50</sub>' for cellular toxicity /  $IC_{50}$  for MERS inhibition) underscored the improved performance of fangchinoline over tetrandrine (Figure 4C, inset). These data support an efficacy of specific bisbenzylisoquinoline alkaloids as agents for targeting MERS-CoV *in vitro*. To assess the ability of the same compounds to inhibit NAADP-evoked  $Ca^{2+}$  release, confocal  $Ca^{2+}$  imaging experiments were performed in human U2OS cells microinjected with NAADP. Preincubation of cells with tetrandrine or fangchinoline ( $10\mu M$ ) inhibited  $Ca^{2+}$  signals triggered by NAADP microinjection ( $69\pm 16\%$  and  $88\pm 3\%$  inhibition for tetrandrine and fangchinoline, respectively), evidencing fangchinoline as an effective inhibitor of both NAADP-evoked  $Ca^{2+}$  release (Figure 4D) and MERS-CoV pseudovirus translocation (Figure 4A&C). No antiviral activity was observed following inhibition of  $IP_3$ - or cADPR-evoked  $Ca^{2+}$  release (Figure 1 in [37]). The inhibition of NAADP-evoked  $Ca^{2+}$  release and MERS-CoV pseudovirus translocation by these compounds was not due to lysosomotropism, as we found no significant decrease in lysosomal  $Ca^{2+}$  content or disruption of lysosomal pH upon addition of these drug (Supplemental Figure 5). Finally, the effects of two other cell permeable

endolysosomal ion channel modulators were examined: the NAADP antagonist ned-19 [38], and the TRPML agonist ML-SA1 [13]. Ned-19 showed poor inhibitory activity in the MERS translocation assays (Figure 4A), which was surprising as it is widely employed as a NAADP blocker. However, in our hands, *trans*-ned-19 (up to ~50 $\mu$ M) also failed to potently inhibit NAADP-evoked Ca<sup>2+</sup> release in either mammalian cells (Figure 4D) or sea urchin homogenate (Figure 4 in [37]), suggesting some caution in interpretation of results obtained with commercially sourced ned-19. The activity of the cell permeable TRPML agonist ML-SA1, which did not modulate MERS-CoV pseudovirus infectivity (Figure 4A), was confirmed as application to mammalian cell lines elicited clear Ca<sup>2+</sup> transients (data not shown).

TPC channels are also regulated by bioactive lipids, including PI(3,5)P<sub>2</sub> [18] and sphingosine for TPC1 [39]. Addition of the PIKfyve inhibitor YM201636 to reduce PI(3,5)P<sub>2</sub> levels, a phosphoinositide which activates TPC channels, decreased MERS-CoV pseudovirus translocation (Supplementary Figure 6A&B). Sphingosine is generated through the action of acid ceramidase (AC, *Asah1*) on ceramide, a product of acid sphingomyelinase (ASM, *Smpd1*) activity (Supplementary Figure 6). Acid sphingomyelinase is required for Ebola infection [40], although the roles of ASM and AC have not been studied in MERS-CoV pseudovirus infectivity. In Huh7 cells exposed to pseudovirus, addition of the antidepressant drugs desipramine or amitriptyline, both of which act as functional inhibitors of ASM [41, 42], inhibited MERS-CoV pseudovirus translocation (Supplementary Figure 6B). Concentration-response curves demonstrated potent inhibition (IC<sub>50</sub>= 796nM for desipramine, IC<sub>50</sub>= 4.8 $\mu$ M for amitriptyline) with little deleterious effects on cellular viability over the concentration range studied (Supplementary Figure 6C). Pharmacological inhibition of AC, to reduce sphingosine levels, also reduced luminescence levels (Supplementary Figure 6B). In contrast, incubation with fumonisin B1, an inhibitor of ceramide synthase enzymes localized in the endoplasmic reticulum, which utilize sphingosine to synthesize ceramide, did not significantly decrease luminescence values. Discrete siRNAs targeting *Smpd1*

or *Asah1* inhibited MERS translocation (Supplementary Figure 6D), and successful knockdown of these enzymes was validated (Supplementary Figure 6E). Therefore, inhibition of enzymes upstream, but not downstream, of the TPC1 activator sphingosine impaired MERS-CoV pseudovirus infectivity. In summary, these data demonstrate dysregulation of known lipid TPC regulators also impeded MERS pseudovirus translocation.

*3.4 How does fangchinoline inhibit MERS translocation?* TPC activity changes both the cytosolic and luminal microenvironment within the acidic  $\text{Ca}^{2+}$  stores. Local, cytoplasmic ion fluxes potentially regulate vesicular dynamics and fusion events [17, 18] to impact MERS-CoV pseudovirus progression through the endolysosomal system. TPC triggered changes in luminal  $\text{Ca}^{2+}$  and pH (51, 52) may also regulate MERS-CoV pseudovirus translocation by regulating proprotein convertase activity needed for proteolytic activation of the spike protein and thereby MERS-CoV fusion and release into the cytoplasm (6, 53). Therefore, we examined the effects of fangchinoline on both these cell biological aspects of MERS-CoV pseudovirus translocation.

First, we assessed the effects of drug incubation on MERS-CoV pseudovirus progression through TPC-positive structures. Treatment of Huh7 cells with fangchinoline (10 $\mu\text{M}$ ) increased MERS particle colocalization with both TPC1-GFP and TPC2-GFP labelled structures (Figure 5A). Quantification of colocalization using Pearson's correlation coefficient [43] from single cell regions of interest in fixed samples showed that fangchinoline treatment increased levels of pixel-to-pixel covariance across MERS and TPC-positive structures (Figure 5A, inset). Analysis of MERS-CoV spike protein colocalization with TPCs using a different algorithm (Manders' coefficient) also demonstrated a similar increase in colocalization after fangchinoline treatment (Figure 5B). These results are suggestive of a drug-evoked blockade of endolysosomal MERS-CoV pseudovirus translocation events. In live cell imaging experiments, it was also evident that fangchinoline treatment impacted the mobility of fluorescent dextran labelled endosomal structures. Single

particle tracking analysis revealed that incubation of cells in fangchinoline, or tetrandrine, decreased the mobility of dextran-labelled endosomal structures (Figure 5C). Impaired movement of TPC1-labelled structures was also seen in cells overexpressing the pore-dead mutant TPC1[L273P]-GFP, but not TPC1-GFP, suggesting that drug-evoked inhibition of TPC1 activity underpinned this effect on endosomal motility (Figure D).

Next, we assessed the effects of drug incubation, or TPC knockdown, on the activity of furin, a  $\text{Ca}^{2+}$ -dependent serine endoprotease. For these experiments, the kinetics of furin-evoked cleavage of a fluorogenic substrate (Boc-RVRR-AMC) was measured in cell lysates under different experimental conditions. In Huh7 cells, pretreatment of cells with fangchinoline (10 $\mu\text{M}$ , 4hr) markedly reduced the rate of substrate cleavage (19.3 $\pm$ 2.5% of control, Figure 6A&B). In contrast, inhibition was not observed during acute drug treatment, demonstrating fangchinoline did not act as a direct furin inhibitor (Figure 6A&B). Similar assays were repeated in HEK293 cells treated with the validated siRNAs against TPC1 or TPC2 (Figure 6C). Knockdown of either TPC isoform impaired furin activity, decreasing the initial rate of substrate cleavage by 59.9 $\pm$ 3.6% (TPC1) or 54.3 $\pm$ 3.0% (TPC2, Figure 6D). These data show that pharmacological or molecular inhibition of TPC function impaired furin activity. Consequently, we tested whether furin overexpression could rescue drug inhibition of MERS-CoV pseudovirus translocation. Overexpression of furin markedly attenuated drug-evoked inhibition of MERS-CoV pseudovirus infectivity in Huh7 cells (Figure 6E). The inhibition observed with tetrandrine and fangchinoline in control experiments (>80% inhibition) was considerably attenuated by transfection with exogenous furin (<30% inhibition, Figure 6E). Overexpression of the serine protease TMPRSS2 to bias MERS-CoV pseudovirus translocation to direct entry via the plasma membrane also rendered both bisbenzylisoquinoline alkaloids ineffective at blocking MERS-CoV pseudovirus infectivity (Figure 6F). The lack of inhibitory action of tetrandrine or fangchinoline after direct cell entry at the plasma membrane rule out the possibility that these compounds act processes

downstream of membrane fusion, including transcription or translation. These data confirm that tetrandrine and fangchinoline act by blocking the trafficking and processing of internalized MERS-CoV pseudovirus particles within the endolysosomal system.

#### 4.0 DISCUSSION

MERS-CoV infections are clinically challenging and are associated with high mortality rates (~30-50%, [2, 3]) due to disease severity and lack of effective pharmacotherapy. Here, we demonstrate that endolysosomal TPCs may represent a druggable host target for MERS-CoV antiviral therapy based on data showing that inhibition of endogenous TPC activity via either molecular or pharmacological methods impaired the cellular translocation of a MERS-CoV pseudovirus. Such findings merit consideration of the role of TPCs as host-factors in supporting MERS-CoV infectivity, and the potential druggability of these ion channels to source novel antivirals. These issues are discussed below.

TPCs are evolutionarily ancient ion channels, resident within the endolysosomal system, where they fulfill homeostatic trafficking functions supporting internalized substrate distribution [13-20]. The mechanistic basis of how these channels regulate endolysosomal trafficking events has been the subject of varied speculation, but it seems clear that perturbing TPC localization, or their activity away from the physiological set-point, disrupts endolysosomal morphology and substrate trafficking. Their importance in subcellular transport extends beyond endogenous substrates, as impactfully highlighted in the context of Ebola infectivity [21]. A role for TPCs in supporting viral translocation is further evidenced here in the context of MERS, another single stranded RNA virus. Investigation of the role of TPCs in other viral infections and in other paradigms of infectious disease, where pathogens exploit or reside within endolysosomal derived organelles is merited.

How do TPCs support MERS passage from cell surface to cytoplasm? Figure 5 shows that TPC activity is necessary to support trafficking events and passage of pseudovirus particles through TPC-positive compartments in the endolysosomal trafficking pathway. Effects on particle progression and processing are likely interdependent: TPCs also regulate furin activity (Figure 6). TPC activity is known to alter both endolysosomal  $\text{Ca}^{2+}$  content and pH [44, 45] and both factors regulate the activity of proprotein convertases (such as furin) required for proteolytic activation of the spike protein, MERS-CoV fusion activity and cytoplasmic translocation [7, 46]. Dysregulation of the luminal microenvironment (pH,  $\text{Ca}^{2+}$ ) owing to changes in TPC activity may then impair MERS-CoV fusion depending on protease levels, or diversity of protease expression, within a given cell type. The inhibitory and non-additive effects of TPC1 (biased toward endosomes) and TPC2 (biased toward lysosomes) knockdown (Figure 2A) suggest that MERS translocation occurs throughout proximal and distal compartments within the acidic  $\text{Ca}^{2+}$  stores. Prior investigations of MERS infectivity suggest fusion and cytoplasmic translocation occurs from early endosomes [8], while more recent studies demonstrate inhibition of cathepsin L, a lysosomal cysteine protease, blocks MERS infectivity [47], both studies consistent with the demonstrated role for both TPC1 and TPC2 (Figure 2). A further conclusion that can be drawn from the current data is that the role of TPCs appears selective: manipulation of TRPML1 function, another 'acidic  $\text{Ca}^{2+}$  store' ion channel, failed to impair MERS-CoV pseudovirus infectivity. These data suggest sub-specialization in endolysosomal channel function and/or trafficking pathways, as TPC inhibition may selectively impair only a subset of transported substrates rather than effect a global disruption of endolysosomal function – a feature that may prove critical in advancing the viability of TPCs as selective drug targets. Selectivity in drug action against TPCs was also evident through a correlation between the extent of inhibition of NAADP-evoked  $\text{Ca}^{2+}$  signals and impairment of MERS translocation (Figure 4), a relationship which is evidenced further in the companion paper [37]. Further drugs that inhibited MERS pseudovirus translocation do not inhibit other intracellular  $\text{Ca}^{2+}$  mobilization pathways (Figure 1 in [37]), even though the role of TPCs in

amplifying  $\text{Ca}^{2+}$  signals through other intracellular  $\text{Ca}^{2+}$  channels beyond the endolysosomal system is well appreciated. In short, the data support a selective, spatially autonomous role for TPCs within acidic organelles in supporting MERS infectivity.

Are TPCs druggable targets for antiviral development? This is a topical issue given renewed interest in repurposing  $\text{Ca}^{2+}$  channel ligands to impair viral infectivity [21, 48, 49], although most attention to date has been directed toward cell surface targets such as voltage-operated  $\text{Ca}^{2+}$  channels (VOCCs). However many VOCC blockers also inhibit NAADP-evoked  $\text{Ca}^{2+}$  release activity in the high micromolar range [50], likely due to the pedigree of the TPC structural blueprint as an antecedent for cell surface voltage-gated channel architecture [33]. TPC blockade may therefore constitute a component of previously described antiviral VOCC antagonist action. The promiscuous pharmacology of TPCs may nevertheless prove a challenge for discovering selective, high affinity TPC ligands. However, the emerging capacity to (i) interrogate cell biological assays that depend on TPC function (such as explored here), (ii) miniaturize NAADP-evoked  $\text{Ca}^{2+}$  release screening platforms (see companion paper, [37]) and (iii) integrate structure-based approaches based upon the recent resolution of TPC crystal structures [51-53], will collectively spur opportunities to identify novel leads and optimizing ligand affinity and selectivity for these channels.

In this context, clear structure-activity correlations emerge from our study of the bisbenzylisoquinoline alkaloids. These compounds are a well-studied natural product group with hundreds of unique compounds described, some displaying activity against other pathogenic eukaryotes [54, 55]. Bisbenzylisoquinoline alkaloids are classified based on the number, type and orientation of ring linkages [56-58]. While the compounds studied here provide only limited insight into the structural diversity of this series, representing compounds with two diphenyl ether linkages differing in their orientation ('head-to-tail' versus 'head-to-head' and 'tail-to-tail'),

nevertheless clear insight into structure-activity relationships impacting MERS translocation/intracellular  $\text{Ca}^{2+}$  release properties was discernable (Figure 4) providing impetus for further structural exploration of the bisbenzylisoquinoline scaffold. This should encompass compounds with differing number of ring linkages (effect of ring flexibility), the position and nature of the ring substitutions, as well as the stereochemistry around the dual asymmetric carbons. We note the potency of tetrandrine against MERS was lower than previously reported for tetrandrine against Ebola (tens of nM *in vitro*, [21]). The improved performance of fangchinoline over tetrandrine in this particular assay supports future optimization of structure activity relationships in this compound series against specific pathogens (Figure 4D). Also noteworthy in our experiments was the efficacy and good selectivity indices seen with the FDA-approved serotonin reuptake inhibitors, amitriptyline and desipramine (Supplementary Figure 6). Further investigation of the interrelationship between the antiviral activity of SSRIs (Supplementary Figure 6, [49]), endolysosomal bioactive lipid content (these compounds act as functional inhibitors of acid sphingomyelinase [41, 42]) and effects on TPC activity is also warranted.

In conclusion, these findings support a unique role for TPCs and NAADP-sensitive  $\text{Ca}^{2+}$  release in MERS infectivity, providing further support for exploration and development of TPC ligands as novel antiviral therapeutics.

**CONFLICTS OF INTEREST** : None.

**ACKNOWLEDGEMENTS.** GG performed and analyzed the experiments shown in Figures 1 through 6. YY prepared pseudovirus for use in all experiments. GG, YY, TFW, FL and JSM collaborated to design experiments. GG and JSM wrote the paper. All authors reviewed the

results, and commented upon the final version of the manuscript. Work in the Marchant Lab is supported by NIH (R01 GM088790) and Regenerative Medicine Minnesota (RMM 11215 DS003).

ACCEPTED MANUSCRIPT

## REFERENCES

- [1] A.M. Zaki, S. van Boheemen, T.M. Bestebroer, A.D. Osterhaus, R.A. Fouchier, Isolation of a novel coronavirus from a man with pneumonia in Saudi Arabia, *N. Engl. J. Med.*, 367 (2012) 1814-1820.
- [2] A. Zumla, D.S. Hui, S. Perlman, Middle East respiratory syndrome, *Lancet*, 386 (2015) 995-1007.
- [3] J.F. Chan, S.K. Lau, K.K. To, V.C. Cheng, P.C. Woo, K.Y. Yuen, Middle East respiratory syndrome coronavirus: another zoonotic betacoronavirus causing SARS-like disease, *Clin. Microbiol. Rev.*, 28 (2015) 465-522.
- [4] A. Zumla, J.F. Chan, E.I. Azhar, D.S. Hui, K.Y. Yuen, Coronaviruses - drug discovery and therapeutic options, *Nat Rev Drug Discov*, 15 (2016) 327-347.
- [5] V.S. Raj, H. Mou, S.L. Smits, D.H. Dekkers, M.A. Muller, R. Dijkman, D. Muth, J.A. Demmers, A. Zaki, R.A. Fouchier, V. Thiel, C. Drosten, P.J. Rottier, A.D. Osterhaus, B.J. Bosch, B.L. Haagmans, Dipeptidyl peptidase 4 is a functional receptor for the emerging human coronavirus-EMC, *Nature*, 495 (2013) 251-254.
- [6] J.E. Park, K. Li, A. Barlan, A.R. Fehr, S. Perlman, P.B. McCray, Jr., T. Gallagher, Proteolytic processing of Middle East respiratory syndrome coronavirus spikes expands virus tropism, *Proc. Natl. Acad. Sci. U. S. A.*, 113 (2016) 12262-12267.
- [7] J.K. Millet, G.R. Whittaker, Host cell entry of Middle East respiratory syndrome coronavirus after two-step, furin-mediated activation of the spike protein, *Proc. Natl. Acad. Sci. U. S. A.*, 111 (2014) 15214-15219.
- [8] C. Burkard, M.H. Verheije, O. Wicht, S.I. van Kasteren, F.J. van Kuppeveld, B.L. Haagmans, L. Pelkmans, P.J. Rottier, B.J. Bosch, C.A. de Haan, Coronavirus cell entry occurs through the endo-/lysosomal pathway in a proteolysis-dependent manner, *PLoS Pathog*, 10 (2014) e1004502.
- [9] C. Burkard, M.H. Verheije, B.L. Haagmans, F.J. van Kuppeveld, P.J. Rottier, B.J. Bosch, C.A. de Haan, ATP1A1-mediated Src signaling inhibits coronavirus entry into host cells, *J. Virol.*, 89 (2015) 4434-4448.
- [10] A.H. de Wilde, D. Jochmans, C.C. Posthuma, J.C. Zevenhoven-Dobbe, S. van Nieuwkoop, T.M. Bestebroer, B.G. van den Hoogen, J. Neyts, E.J. Snijder, Screening of an FDA-approved compound library identifies four small-molecule inhibitors of Middle East respiratory syndrome coronavirus replication in cell culture, *Antimicrob. Agents Chemother.*, 58 (2014) 4875-4884.
- [11] J.S. Marchant, S. Patel, Two-pore channels at the intersection of endolysosomal membrane traffic, *Biochem. Soc. Trans.*, 43 (2015) 434-441.
- [12] D. Shen, X. Wang, H. Xu, Pairing phosphoinositides with calcium ions in endolysosomal dynamics: phosphoinositides control the direction and specificity of membrane trafficking by regulating the activity of calcium channels in the endolysosomes, *Bioessays*, 33 (2011) 448-457.

- [13] D. Shen, X. Wang, X. Li, X. Zhang, Z. Yao, S. Dibble, X.P. Dong, T. Yu, A.P. Lieberman, H.D. Showalter, H. Xu, Lipid storage disorders block lysosomal trafficking by inhibiting a TRP channel and lysosomal calcium release, *Nature communications*, 3 (2012) 731.
- [14] Y. Lin-Moshier, M.V. Keebler, R. Hooper, M.J. Boulware, X. Liu, D. Churamani, M.E. Abood, T.F. Walseth, E. Brailoiu, S. Patel, J.S. Marchant, The Two-pore channel (TPC) interactome unmasks isoform-specific roles for TPCs in endolysosomal morphology and cell pigmentation, *Proc. Natl. Acad. Sci. U. S. A.*, 111 (2014) 13087-13092.
- [15] M. Ruas, K. Rietdorf, A. Arredouani, L.C. Davis, E. Lloyd-Evans, H. Koegel, T.M. Funnell, A.J. Morgan, J.A. Ward, K. Watanabe, X.T. Cheng, G.C. Churchill, M.X. Zhu, F.M. Platt, G.M. Wessel, J. Parrington, A. Galione, Purified TPC Isoforms Form NAADP Receptors with Distinct Roles for Ca<sup>2+</sup> Signaling and Endolysosomal Trafficking, *Curr. Biol.*, 20 (2010) 703-709.
- [16] M. Ruas, K.T. Chuang, L.C. Davis, A. Al-Douri, P.W. Tynan, R. Tunn, L. Teboul, A. Galione, J. Parrington, TPC1 has two variant isoforms, and their removal has different effects on endolysosomal functions compared to loss of TPC2, *Mol. Cell. Biol.*, 34 (2014) 3981-3992.
- [17] C. Grimm, L.M. Holdt, C.C. Chen, S. Hassan, C. Muller, S. Jors, H. Cuny, S. Kissing, B. Schroder, E. Butz, B. Northoff, J. Castonguay, C.A. Lubber, M. Moser, S. Spahn, R. Lullmann-Rauch, C. Fendel, N. Klugbauer, O. Griesbeck, A. Haas, M. Mann, F. Bracher, D. Teupser, P. Saftig, M. Biel, C. Wahl-Schott, High susceptibility to fatty liver disease in two-pore channel 2-deficient mice, *Nature communications*, 5 (2014) 4699.
- [18] X. Wang, X. Zhang, X.P. Dong, M. Samie, X. Li, X. Cheng, A. Goschka, D. Shen, Y. Zhou, J. Harlow, M.X. Zhu, D.E. Clapham, D. Ren, H. Xu, TPC proteins are phosphoinositide-activated sodium-selective ion channels in endosomes and lysosomes, *Cell*, 151 (2012) 372-383.
- [19] Y. Lu, B.X. Hao, R. Graeff, C.W. Wong, W.T. Wu, J. Yue, Two pore channel 2 (TPC2) inhibits autophagosomal-lysosomal fusion by alkalinizing lysosomal pH, *J. Biol. Chem.*, 288 (2013) 24247-24263.
- [20] L. Hockey, B.S. Kilpatrick, E.R. Eden, Y. Lin-Moshier, G.C. Brailoiu, E. Brailoiu, C.E. Futter, A.H. Schapira, J.S. Marchant, S. Patel, Dysregulation of lysosomal morphology by pathogenic LRRK2 is corrected by two-pore channel inhibition, *J Cell Science*, 128 (2015) 232-238.
- [21] Y. Sakurai, A.A. Kolokoltsov, C.C. Chen, M.W. Tidwell, W.E. Bauta, N. Klugbauer, C. Grimm, C. Wahl-Schott, M. Biel, R.A. Davey, Ebola virus. Two-pore channels control Ebola virus host cell entry and are drug targets for disease treatment, *Science*, 347 (2015) 995-998.
- [22] J.A. Simmons, R.S. D'Souza, M. Ruas, A. Galione, J.E. Casanova, J.M. White, Ebolavirus Glycoprotein Directs Fusion through NPC1+ Endolysosomes, *J. Virol.*, 90 (2016) 605-610.
- [23] Y. Lin-Moshier, T.F. Walseth, D. Churamani, S.M. Davidson, J.T. Slama, R. Hooper, E. Brailoiu, S. Patel, J.S. Marchant, Photoaffinity labeling of nicotinic acid adenine dinucleotide phosphate (NAADP) targets in mammalian cells, *J. Biol. Chem.*, 287 (2012) 2296-2307.
- [24] E. Brailoiu, D. Churamani, X. Cai, M.G. Schrlau, G.C. Brailoiu, X. Gao, R. Hooper, M.J. Boulware, N.J. Dun, J.S. Marchant, S. Patel, Essential requirement for two-pore channel 1 in NAADP-mediated calcium signaling, *J. Cell Biol.*, 186 (2009) 201-209.

- [25] E. Brailoiu, T. Rahman, D. Churamani, D.L. Prole, G.C. Brailoiu, R. Hooper, C.W. Taylor, S. Patel, An NAADP-gated two-pore channel targeted to the plasma membrane uncouples triggering from amplifying  $\text{Ca}^{2+}$  signals, *J. Biol. Chem.*, 285 (2010) 38511-38516.
- [26] G. Zhao, L. Du, C. Ma, Y. Li, L. Li, V.K. Poon, L. Wang, F. Yu, B.J. Zheng, S. Jiang, Y. Zhou, A safe and convenient pseudovirus-based inhibition assay to detect neutralizing antibodies and screen for viral entry inhibitors against the novel human coronavirus MERS-CoV, *Virology journal*, 10 (2013) 266.
- [27] Y. Yang, L. Du, C. Liu, L. Wang, C. Ma, J. Tang, R.S. Baric, S. Jiang, F. Li, Receptor usage and cell entry of bat coronavirus HKU4 provide insight into bat-to-human transmission of MERS coronavirus, *Proc. Natl. Acad. Sci. U. S. A.*, 111 (2014) 12516-12521.
- [28] K.M. Hussain, K.L. Leong, M.M. Ng, J.J. Chu, The essential role of clathrin-mediated endocytosis in the infectious entry of human enterovirus 71, *J. Biol. Chem.*, 286 (2011) 309-321.
- [29] Z. Qian, S.R. Dominguez, K.V. Holmes, Role of the spike glycoprotein of human Middle East respiratory syndrome coronavirus (MERS-CoV) in virus entry and syncytia formation, *PLoS ONE*, 8 (2013) e76469.
- [30] X. Li, A.G. Garrity, H. Xu, Regulation of membrane trafficking by signalling on endosomal and lysosomal membranes, *J Physiol*, 591 (2013) 4389-4401.
- [31] C. Grimm, S. Hassan, C. Wahl-Schott, M. Biel, Role of TRPML and two-pore channels in endolysosomal cation homeostasis, *J. Pharmacol. Exp. Ther.*, 342 (2012) 236-244.
- [32] P.J. Calcraft, M. Ruas, Z. Pan, X. Cheng, A. Arredouani, X. Hao, J. Tang, K. Rietdorf, L. Teboul, K.T. Chuang, P. Lin, R. Xiao, C. Wang, Y. Zhu, Y. Lin, C.N. Wyatt, J. Parrington, J. Ma, A.M. Evans, A. Galione, M.X. Zhu, NAADP mobilizes calcium from acidic organelles through two-pore channels, *Nature*, 459 (2009) 596-600.
- [33] T. Rahman, X. Cai, G.C. Brailoiu, M.E. Abood, E. Brailoiu, S. Patel, Two-pore channels provide insight into the evolution of voltage-gated  $\text{Ca}^{2+}$  and  $\text{Na}^+$  channels, *Sci Signal*, 7 (2014) ra109.
- [34] M. Ruas, L.C. Davis, C.C. Chen, A.J. Morgan, K.T. Chuang, T.F. Walseth, C. Grimm, C. Garnham, T. Powell, N. Platt, F.M. Platt, M. Biel, C. Wahl-Schott, J. Parrington, A. Galione, Expression of  $\text{Ca}^{2+}$ -permeable two-pore channels rescues NAADP signalling in TPC-deficient cells, *EMBO J.*, 34 (2015) 1743-1758.
- [35] A. Jha, M. Ahuja, S. Patel, E. Brailoiu, S. Muallem, Convergent regulation of the lysosomal two-pore channel-2 by  $\text{Mg}^{2+}$ , NAADP,  $\text{PI}(3,5)\text{P}_2$  and multiple protein kinases, *EMBO J.*, 33 (2014) 501-511.
- [36] X. Zong, M. Schieder, H. Cuny, S. Fenske, C. Gruner, K. Rotzer, O. Griesbeck, H. Harz, M. Biel, C. Wahl-Schott, The two-pore channel TPCN2 mediates NAADP-dependent  $\text{Ca}^{2+}$ -release from lysosomal stores, *Pflugers Arch.*, 458 (2009) 891-899.
- [37] G. Gunaratne, M.E. Johns, T.F. Walseth, J.S. Marchant, A screening campaign in sea urchin egg homogenate as a platform for discovering modulators of NAADP-dependent  $\text{Ca}^{2+}$  signals in human cells, *Companion paper*, (2018).

- [38] E. Naylor, A. Arredouani, S.R. Vasudevan, A.M. Lewis, R. Parkesh, A. Mizote, D. Rosen, J.M. Thomas, M. Izumi, A. Ganesan, A. Galione, G.C. Churchill, Identification of a chemical probe for NAADP by virtual screening, *Nat Chem Biol*, 5 (2009) 220-226.
- [39] D. Hoglinger, P. Haberkant, A. Aguilera-Romero, H. Riezman, F.D. Porter, F.M. Platt, A. Galione, C. Schultz, Intracellular sphingosine releases calcium from lysosomes, *eLife*, 4 (2015).
- [40] M.E. Miller, S. Adhikary, A.A. Kolokoltsov, R.A. Davey, Ebolavirus requires acid sphingomyelinase activity and plasma membrane sphingomyelin for infection, *J. Virol.*, 86 (2012) 7473-7483.
- [41] E. Gulbins, M. Palmada, M. Reichel, A. Luth, C. Bohmer, D. Amato, C.P. Muller, C.H. Tischbirek, T.W. Groemer, G. Tabatabai, K.A. Becker, P. Tripal, S. Staedtler, T.F. Ackermann, J. van Brederode, C. Alzheimer, M. Weller, U.E. Lang, B. Kleuser, H. Grassme, J. Kornhuber, Acid sphingomyelinase-ceramide system mediates effects of antidepressant drugs, *Nat. Med.*, 19 (2013) 934-938.
- [42] J. Kornhuber, M. Muehlbacher, S. Trapp, S. Pechmann, A. Friedl, M. Reichel, C. Muhle, L. Terfloth, T.W. Groemer, G.M. Spitzer, K.R. Liedl, E. Gulbins, P. Tripal, Identification of novel functional inhibitors of acid sphingomyelinase, *PLoS ONE*, 6 (2011) e23852.
- [43] K.W. Dunn, M.M. Kamocka, J.H. McDonald, A practical guide to evaluating colocalization in biological microscopy, *Am J Physiol Cell Physiol*, 300 (2011) C723-742.
- [44] A.J. Morgan, A. Galione, Fertilization and nicotinic acid adenine dinucleotide phosphate induce pH changes in acidic Ca(2+) stores in sea urchin eggs, *J. Biol. Chem.*, 282 (2007) 37730-37737.
- [45] F. Cosker, N. Cheviron, M. Yamasaki, A. Menteyne, F.E. Lund, M.J. Moutin, A. Galione, J.M. Cancela, The ecto-enzyme CD38 is a nicotinic acid adenine dinucleotide phosphate (NAADP) synthase that couples receptor activation to Ca<sup>2+</sup> mobilization from lysosomes in pancreatic acinar cells, *J. Biol. Chem.*, 285 (2010) 38251-38259.
- [46] G. Thomas, Furin at the cutting edge: from protein traffic to embryogenesis and disease, *Nature reviews. Molecular cell biology*, 3 (2002) 753-766.
- [47] N. Zhou, T. Pan, J. Zhang, Q. Li, X. Zhang, C. Bai, F. Huang, T. Peng, J. Zhang, C. Liu, L. Tao, H. Zhang, Glycopeptide Antibiotics Potently Inhibit Cathepsin L in the Late Endosome/Lysosome and Block the Entry of Ebola Virus, Middle East Respiratory Syndrome Coronavirus (MERS-CoV), and Severe Acute Respiratory Syndrome Coronavirus (SARS-CoV), *J. Biol. Chem.*, 291 (2016) 9218-9232.
- [48] G. Gehring, K. Rohrmann, N. Atenchong, E. Mittler, S. Becker, F. Dahlmann, S. Pohlmann, F.W. Vondran, S. David, M.P. Manns, S. Ciesek, T. von Hahn, The clinically approved drugs amiodarone, dronedarone and verapamil inhibit filovirus cell entry, *J. Antimicrob. Chemother.*, 69 (2014) 2123-2131.
- [49] L.M. Johansen, L.E. DeWald, C.J. Shoemaker, B.G. Hoffstrom, C.M. Lear-Rooney, A. Stossel, E. Nelson, S.E. Delos, J.A. Simmons, J.M. Grenier, L.T. Pierce, H. Pajouhesh, J. Lehar, L.E. Hensley, P.J. Glass, J.M. White, G.G. Olinger, A screen of approved drugs and

molecular probes identifies therapeutics with anti-Ebola virus activity, *Science translational medicine*, 7 (2015) 290ra289.

[50] A.A. Genazzani, M. Mezna, D.M. Dickey, F. Michelangeli, T.F. Walseth, A. Galione, Pharmacological properties of the  $Ca^{2+}$ -release mechanism sensitive to NAADP in the sea urchin egg, *Br. J. Pharmacol.*, 121 (1997) 1489-1495.

[51] J. Guo, W. Zeng, Q. Chen, C. Lee, L. Chen, Y. Yang, C. Cang, D. Ren, Y. Jiang, Structure of the voltage-gated two-pore channel TPC1 from *Arabidopsis thaliana*, *Nature*, 531 (2016) 196-201.

[52] A.F. Kintzer, R.M. Stroud, Structure, inhibition and regulation of two-pore channel TPC1 from *Arabidopsis thaliana*, *Nature*, 531 (2016) 258-262.

[53] J. She, J. Guo, Q. Chen, W. Zeng, Y. Jiang, X.C. Bai, Structural insights into the voltage and phospholipid activation of the mammalian TPC1 channel, *Nature*, 556 (2018) 130-134.

[54] S.J. Marshall, P.F. Russell, C.W. Wright, M.M. Anderson, J.D. Phillipson, G.C. Kirby, D.C. Warhurst, P.L. Schiff, Jr., In vitro antiplasmodial, antiamebic, and cytotoxic activities of a series of bisbenzylisoquinoline alkaloids, *Antimicrob. Agents Chemother.*, 38 (1994) 96-103.

[55] S. Sureram, S.P. Senadeera, P. Hongmanee, C. Mahidol, S. Ruchirawat, P. Kittakoop, Antimycobacterial activity of bisbenzylisoquinoline alkaloids from *Tiliacora triandra* against multidrug-resistant isolates of *Mycobacterium tuberculosis*, *Bioorg. Med. Chem. Lett.*, 22 (2012) 2902-2905.

[56] K.T. Buck, The Bisbenzylisoquinoline alkaloids, in: A. Brossi (Ed.) *The Alkaloids*, Academic Press 1987, pp. 1-202.

[57] K.P. Guha, B. Mukherjee, R. Mukherjee, Bisbenzylisoquinoline alkaloids - a review, *J. Nat. Prod.*, 42 (1979) 1-84.

[58] P.L. Schiff Jr., Bisbenzylisoquinoline alkaloids, *J. Nat. Prod.*, 54 (1991) 645-749.

## FIGURE LEGENDS

**Figure 1. MERS-pseudovirus assay validation.** **A**, *Top*, schematic representation of MERS-pseudovirus infection pathway, highlighting individual processes during MERS translocation (binding, internalization, trafficking, release) that are targets for pharmacotherapy. MERS particle association with DPP4 (the host entry receptor) is followed by DPP4-dependent internalization and trafficking through acidic  $\text{Ca}^{2+}$  stores and release of luciferase-encoding RNA into the cytoplasm of infected cells after fusion with internal membranes. Note, the pseudovirus translocation assay used for these experiments is replication defective and reports only virus translocation. *Bottom*, trafficking events through the endolysosomal system are regulated by the activity of ion channels resident within these acidic  $\text{Ca}^{2+}$  stores, including members of the TRPML (activated by  $\text{PI}(3,5)\text{P}_2$ ) and TPC family (activated by NAADP and  $\text{PI}(3,5)\text{P}_2$ ). **B**, Effect of drug incubation (spanning 1hr prior to pseudovirus addition and for a 5hr co-incubation after) on MERS infectivity measured in terms of luminescence intensity measured 3 days post-infection. Drug concentrations were: ouabain (100nM), chlorpromazine (10 $\mu\text{M}$ ), chloroquine (10 $\mu\text{M}$ ),  $\text{NH}_4\text{Cl}$  (5mM), BAPTA-AM (10 $\mu\text{M}$ ), bafilomycin (100nM). Pseudovirus infectivity was unaffected by the presence of DMSO (0.1%) as drug vehicle. **C**, Delayed exposure to bafilomycin ( $\dagger$ , 6hr exposure, 5hr after pseudovirus addition) attenuated the inhibitory effect of bafilomycin (100nM) on MERS infectivity. Data from each experiment are normalized to untreated control samples, and values represent mean  $\pm$  SEM from three or more independent experiments. p-values, \*\*  $p < 0.01$ , \*  $p < 0.05$ , calculated relative to DMSO sample.

**Figure 2. Knockdown of TPCs inhibits MERS pseudovirus translocation.** **A**, Effect of construct overexpression or endogenous protein knockdown (grey bars), on MERS infectivity. All experiments were done in HEK293 cells co-transfected with the MERS entry receptor DPP4, which enhanced infectivity (black). p-values: \*\*  $p < 0.01$ , \*  $p < 0.05$ . **B**, *Top*, representative gel

images of RT-PCR samples from knockdown experiments. Samples from control cells ('c') and cells treated with dual control siRNAs and individual channel targeting siRNAs (gene of interest, GOI). *Bottom*, cumulative measurements quantifying knockdown of TPC1 (left), TPC2 (middle), and TRPML1 (right) as determined by densitometry analysis of RT-PCR samples after electrophoresis. Samples are normalized to GAPDH loading control. cells. p-values: \*\*  $p < 0.01$ , relative to control siRNA#1.

**Figure 3. MERS-CoV spike protein colocalizes with endolysosomal ion channel positive structures.** Huh7 cells were transfected with TPC1-GFP (top, green), TPC2-GFP (middle, green) and GFP-TRPML1 (bottom, green) and subsequently infected with MERS-pseudovirus (red). Cells were fixed, immunostained for MERS-CoV spike protein (spike-AF555) and visualized by confocal microscopy. White boxes in overlay panel (right) show enlarged regions to assess colocalization between the red and green channel. Scalebars, 10 $\mu$ m (left column) and 1 $\mu$ m (inset, right).

**Figure 4. Pharmacological blockade of MERS pseudovirus infectivity. A,** Single-concentration drug screening (10 $\mu$ M) to identify ion channel modulators that inhibit MERS pseudovirus translocation. Huh7 cells were treated with indicated drugs for 6hrs, starting 1hr prior to incubation with MERS pseudovirus (i.e. a 5hr co-incubation). Drugs represent known modulators of intracellular TRPML (ML-SA1) and TPC channels (ned-19, voltage-operated channel blockers), as well as a series of structurally related bisbenzylisoquinolines encompassing the known TPC blocker tetrandrine. Screened bisbenzylisoquinolines comprised two groupings: tubocurarine-like compounds (light dashed) and tetrandrine-like compounds (heavy dashed). p-values, \*\*  $p < 0.01$ , \*  $p < 0.05$ . **B,** Structures representing the two groups of bisbenzylisoquinolines highlighted in 'A'. 3D conformers were downloaded from PubChem and displayed in PubChem 3D viewer v2.0. **C,** Complete concentration response relationships for

inhibition of MERS translocation by fangchinoline, tetrandrine, berbamine or ned-19. Inset, selectivity index ( $CC_{50}$  for cellular toxicity/  $IC_{50}$  for pseudovirus translocation) for indicated compounds. **D**, Inhibition of  $Ca^{2+}$  signals in U2OS cells microinjected with NAADP (100nM pipette concentration) after drug treatment (0.1% DMSO, 50 $\mu$ M ned-19, 10 $\mu$ M tetrandrine, 10 $\mu$ M fangchinoline, 10min preincubation). Traces represent average of 3 independent injections, error bars represent S.E.M.

**Figure 5. TPC1 activity regulates endosomal motility and MERS pseudovirus**

**translocation through acidic  $Ca^{2+}$  stores. A**, Effect of incubation with fangchinoline (10 $\mu$ M, right) on colocalization between TPC1 (top) or TPC2 (bottom, green channels) with MERS CoV spike protein (red) in Huh7 cells. Representative cells used to calculate Pearson's correlation coefficient (inset, [43]) are shown. **B**, Colocalization analysis in immunofluorescence samples assessed using Manders' overlap co-efficient [43], in TPC1- and TPC2- expressing cells treated with vehicle (DMSO, solid) and cells treated with fangchinoline (10 $\mu$ M, hatched bars), p-values: \*\*  $p < 0.01$ , \*  $p < 0.05$ . **C**, Trajectory plots representing dynamics of individual TPC1-positive structures in Huh7 cells. Traces represent projections of 20 randomly selected particles, imaged over a 1 minute timeframe under different experimental conditions: control (untransfected), vehicle treated (DMSO, 0.1%), drug treated (10 $\mu$ M, 1hr pretreatment), TPC1-GFP or TPC1[L273P]-GFP transfected. **D**, Cumulative quantification of total distance traveled from point of origin by endosomes in Huh7 cells treated with the indicated compounds, p-values: \*\*  $p < 0.01$ , \*  $p < 0.05$ .

**Figure 6. Pharmacological and molecular inhibition of TPCs reduces furin activity. A**,

Huh7 cells were treated with vehicle or fangchinoline (10 $\mu$ M), lysates were harvested from cells, and furin activity was assessed using fluorogenic substrate, Boc-RVRR-AMC. Drug was added either 4hr prior to harvesting (pretreated) or immediately before addition of substrate (acute).

Representative traces are shown, linear range used to calculate furin substrate cleavage (RFU/min) is shown using dashed lines. **B**, Quantification of cumulative data set of furin activity in pharmacologically treated Huh7 lysates. p-values, \*\*  $p < 0.01$  relative to DMSO control **C**, HEK293 cells were treated with the indicated siRNAs, lysates were collected and assayed for furin activity. Representative traces are shown, with linear range of substrate cleavage denoted using dashed lines. **D**, Quantification of cumulative data set of furin activity using siRNA treated HEK293 cells, p-values: \*\*  $p < 0.01$ , relative to non-targeting siRNA treated samples. **E**, Effect of furin or TMPRSS2 overexpression on pharmacological blockade of MERS-pseudovirus infectivity, p-values: \*\*  $p < 0.01$  relative to empty vector transfected DMSO treated controls, ##  $p < 0.01$  relative to empty vector transfected samples treated with tetrandrine or fangchinoline. **F**, Effect of tetrandrine or fangchinoline treatment on Huh7 cells overexpressing TMPRSS2.

Figure 1

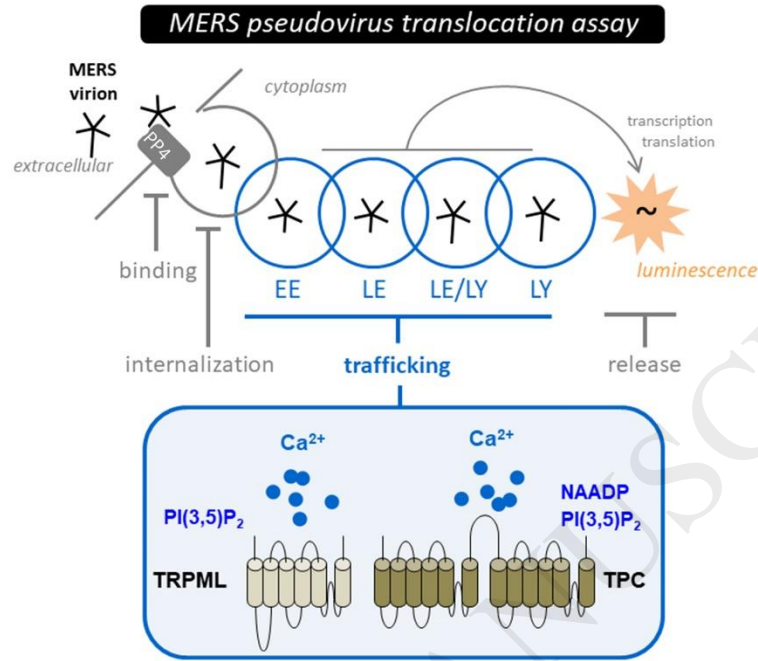
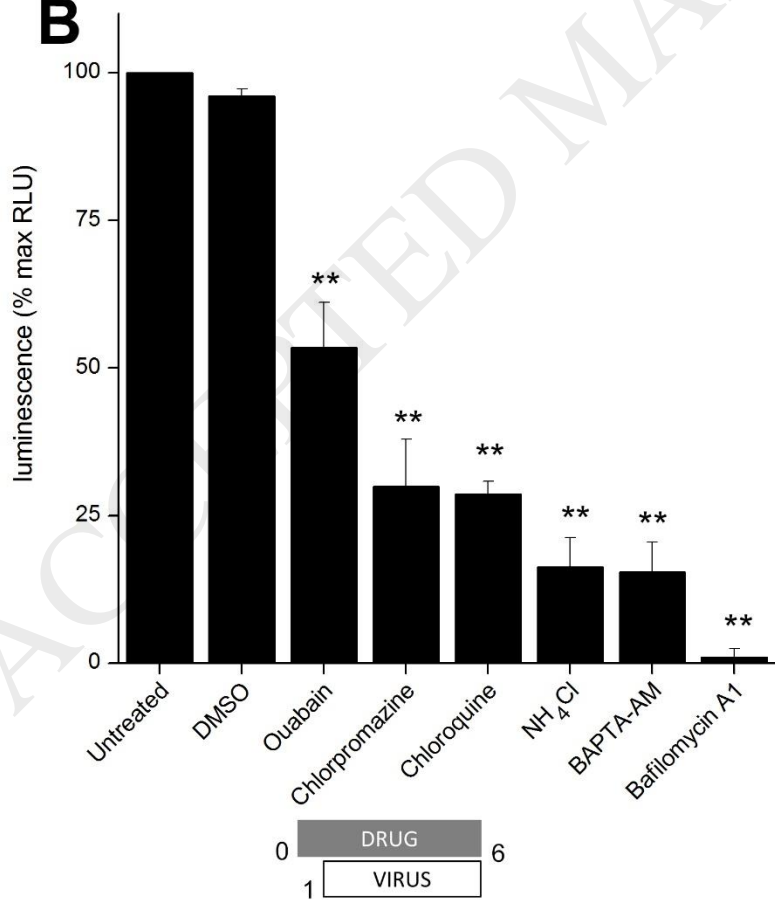
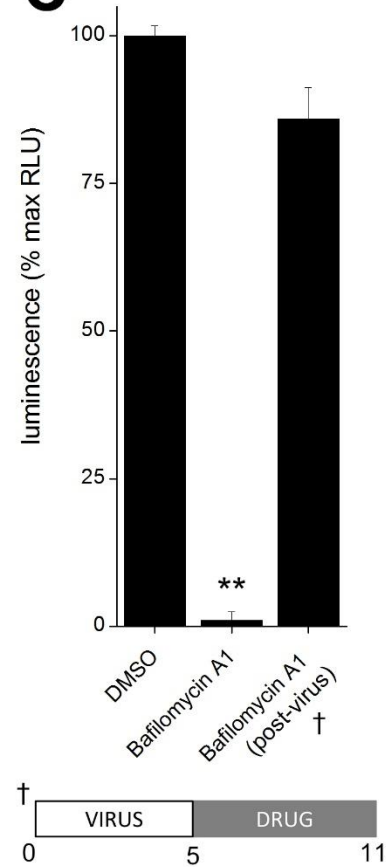
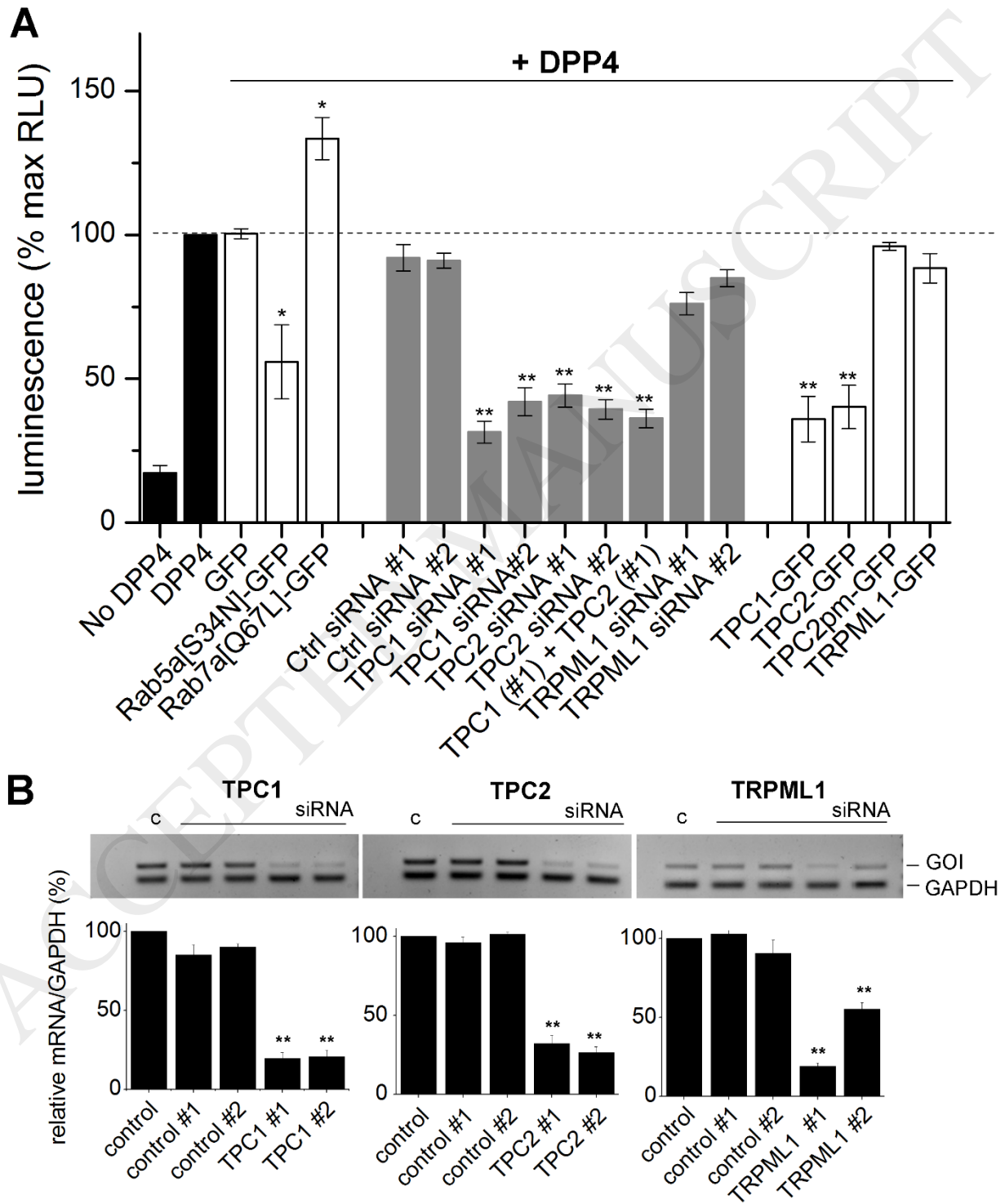
**A****B****C**

Figure 2



ACCEPTED MANUSCRIPT

Figure 3

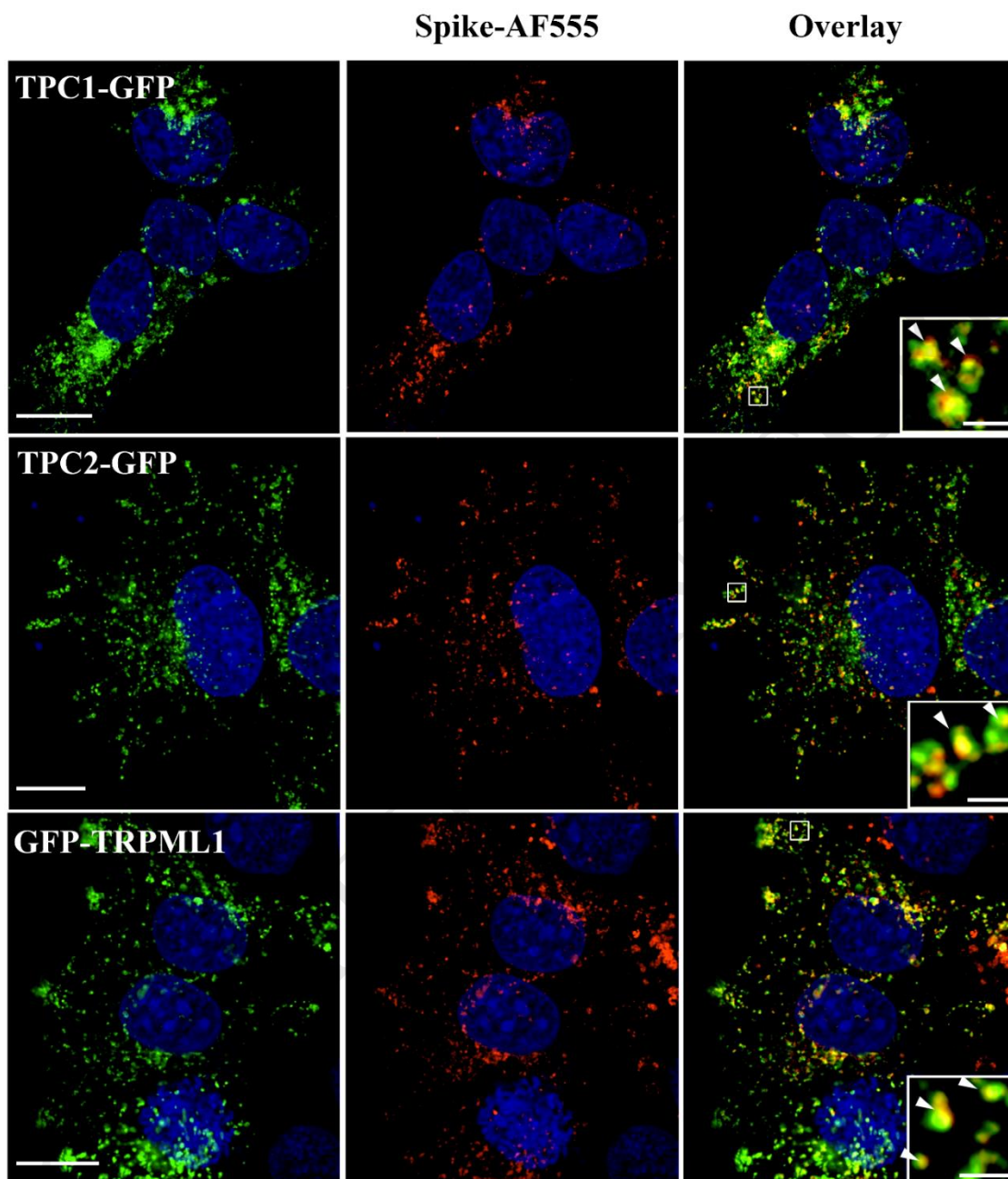


Figure 4

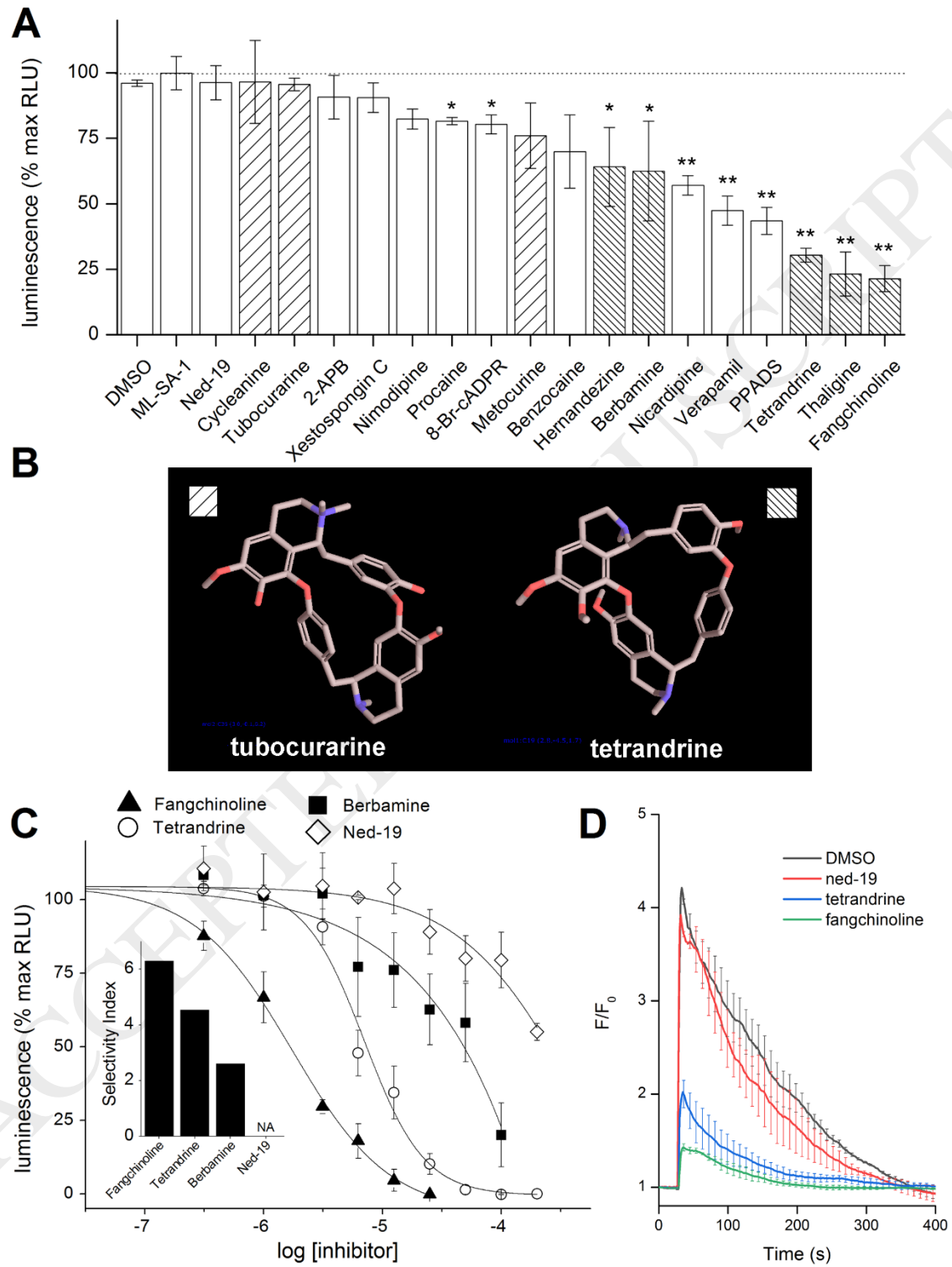


Figure 5

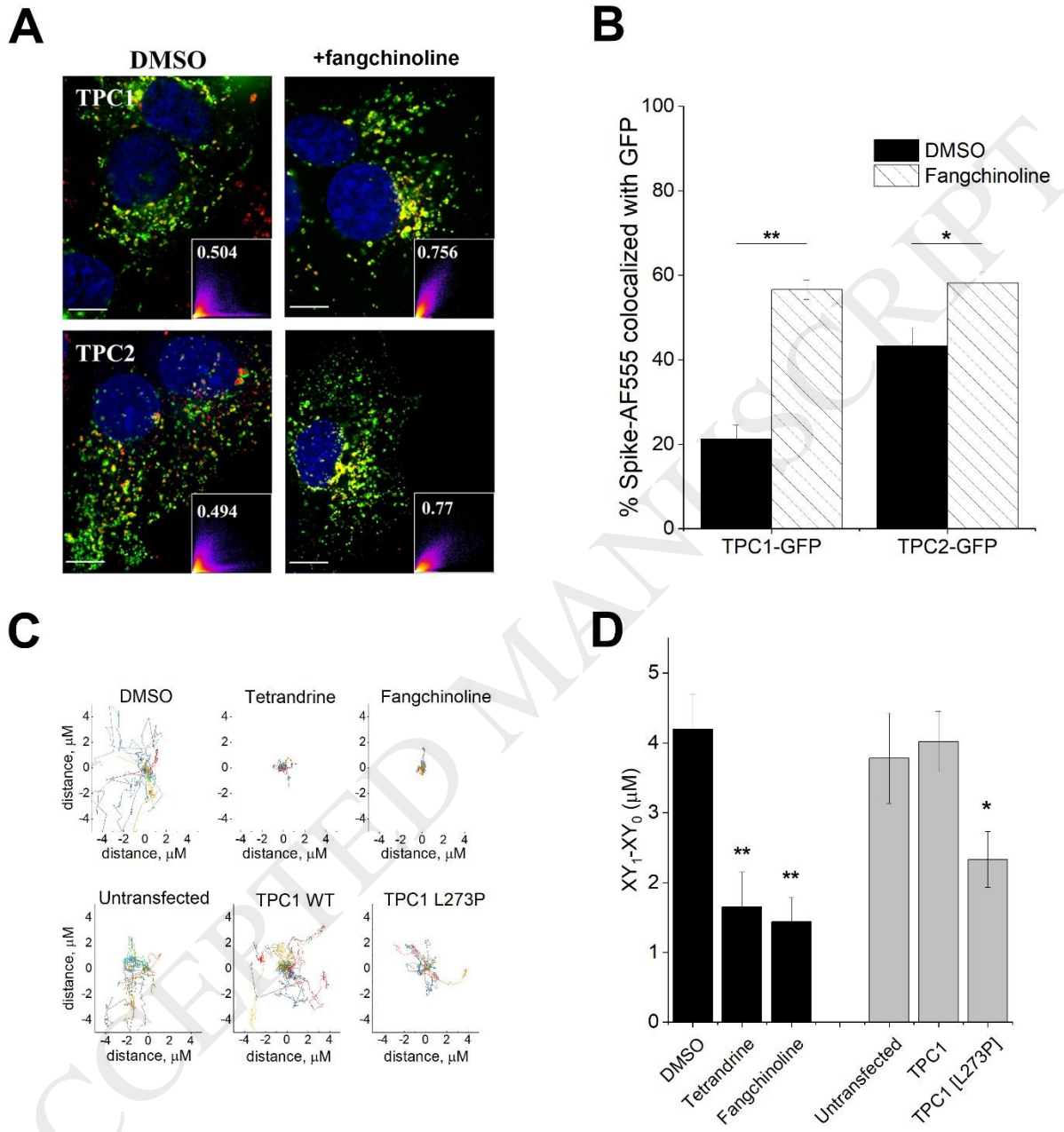


Figure 6

